www.ietdl.org

Published in IET Microwaves, Antennas & Propagation
Received on 20th December 2012
Revised on 16th April 2013
Accepted on 19th May 2013
doi: 10.1049/iet-map.2012.0717

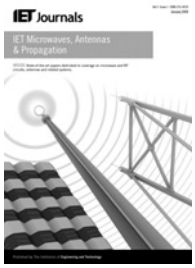

ISSN 1751-8725

Intra-volume, centralised array concept for improved public-safety communications

William F. Young[1], David W. Matolak[2], Nicholas Bikhazi[3], Christopher Holloway[1], Galen Koepke[1], Helge Fielitz[4], Qiong Wu[5], Qian Zhang[6]

[1]*RF Fields Group, The National Institute of Standards and Technology, Broadway, Boulder 80305, Colorado, USA*
[2]*Department of Electrical Engineering, University of South Carolina, 3A28 Swearingen Engineering Center, 301 South Main Street, District of Columbia, SC 29208, USA*
[3]*Sandia National Laboratories, Albuquerque, P.O. Box 5800, MS 0812 87185-0812, New Mexico, USA*
[4]*Hamburg University of Technology, Harburger Schloßstraße 20, Hamburg 21079, Germany*
[5]*Apple, Inc., 1 Infinite Loop, Cupertino 95014, California, USA*
[6]*InterDigital Corp, 781 Third Avenue, King of Prussia 19406, Pennsylvania, USA*
E-mail: wfy@boulder.nist.gov

Abstract: The author report on the testing and measurements of an intra-volume centralised array concept suitable for public-safety communications in buildings. The centralised array concept refers to the use of several small communication devices that are arbitrarily placed in an area and hence create a real-time communication network. The overall concept is to use randomly located (or arbitrarily placed) wireless devices in a coordinated manner in order to increase the radio-frequency signal level otherwise at unreachable locations. In a typical *ad-hoc* network, the transmission range of any communication link in that path is limited. We seek to extend the radio-frequency coverage within the array volume by using two or more nodes as elements of a phased array. The measurement results presented here, collected in real-world environments, along with simulations based on real-world data demonstrate that the centralised array technique can provide useful gain, up to 10 dB with only four elements. Both the measurements and simulations also indicate a typical gain of 2 to 6 dB, using only two elements. Analysis of the phase indicates a phase alignment of ±45° achieves within 1 dB of the maximum gain.

1 Introduction

When emergency responders enter large structures (apartment and office buildings, sports stadiums, malls, hotels, convention centres, warehouses etc.) radio communication to individuals on the outside is often impaired. Mobile-radio signal strength is reduced because of attenuation caused by propagation through the building materials and scattering by the building structural members [1–7]. In addition, a large amount of signal variability may be encountered because of multipath reflections throughout the structures, which can cause severe signal degradation. Here, we report on a project conducted by the National Institute of Standards and Technology (NIST) to investigate the concept of a wireless centralised array to help mitigate communications problems faced by public-safety personnel (firefighters, police and emergency medical personnel) in disaster situations involving large building structures [The project was sponsored by the Department of Justice Community Oriented Policing Services (COPSs) program through the NIST Public Safety Communications Research Laboratory (PSCRL)]. This project focuses on 750 MHz and 2.4 GHz. The 750 MHz band is currently of interest, because the FCC is in the process of allocating spectrum between 764 and 776 MHz for a nationwide, next-generation interoperable broadband network for use by the public-safety community [8, 9] [We were granted a Federal Communications Commission (FCC) temporary approval to broadcast at 750 MHz for a series of propagation studies; radio-frequency propagation behaviour does not differ significantly between 750 MHz and frequencies in the 764–776 MHz band]. The 2.4 GHz band is a widely used industrial, scientific and medical band [10, 11].

The 'intra-volume' wireless centralised array concept tested here is neither a traditional *ad-hoc* wireless network nor a traditional phased antenna array. In a traditional *ad-hoc* wireless network, one key process is to establish node-by-node connectivity for relaying messages [12, 13]. In that case, the transmission range of any communication link in that relay is limited (a node refers to one communication device). A traditional phased array (when operating in transmit mode) assumes the receiving location is in the far-field of the complete array volume. Several papers cover the concept of using distributed wireless nodes as a phased array from a signal processing perspective, for example [14–16], typically to provide 'reach back' to a distant location. Although our centralised wireless array is a type of distributed array, we are not trying to establish a

communication link with a node that is in the far-field of the array volume, such as a distant base station. Rather, we are connecting to a node that is 'within' the array volume, for example, a node within a building containing the wireless devices.

The main contributions in this paper are: (i) the introduction of an intra-volume centralised [*ad-hoc* (Our array is '*ad-hoc*' in the sense that transmitting or receiving nodes are spatially distributed in an arbitrary manner, but not in the sense of the absence of any centralised control – we therefore use the term 'centralised' to avoid confusion.)] wireless array, (ii) measurement results from two real-world experiments (a laboratory basement and an urban office/store setting) that demonstrate the performance benefits of the concept and (iii) a simulation approach that corroborates the intra-volume array performance. The remainder of this paper is organised as follows. Section 2 describes the signal optimisation process and measurement approach, Section 3 describes the test setup and environments, Section 4 discusses measurement and simulation results and Section 5 provides conclusions.

2 Signal processing and measurement methods

2.1 General description

The idea of arbitrarily located wireless devices used in an intelligent and coordinated fashion for emergency responders was initially investigated in [17–19]. These efforts started as an optimisation problem, with infinitesimal dipoles in the presence of several boundary configurations, and used simulation studies to investigate the potential gains available. Optimisation here means the selection of complex weightings, that is, phase and amplitude, so that the transmitted signals from the array nodes arrive co-phased at the receive node, with amplitude levels that maximise the aggregate received power. In the communication literature, with the inclusion of additive noise, this is known as maximal ratio combining (MRC) [11, 20] at the receiver and maximal ratio transmission (MRT) [20, 21] when alignments are made at multiple transmitters.

Results in our earlier work identify some key considerations in constructing a field-deployable implementation. First, diminishing returns in total received power occur once the array contains a small number of transmitters, approximately four for the MRT case and 6–8 for the co-phased case (i.e. phase only weighting) [23, 24]. In the communications field, this co-phasing is also known as equal-gain combining (EGC), [25, 26] and equal-gain transmission (EGT) [20, 21]. (Henceforth, we will use the terminology MRC, MRT, EGC and EGT.) Second, for this same small number of transmitters, the modified directivity results [see (11) in [18]] are not significantly different for the MRT and EGT results [17–19]. Thus, we focus on obtaining the EGT and EGC results, with the recognition that the algorithm also provides a reasonable approximation of the MRT modified directivity. An important observation made in [19] is that the EGT process is not highly sensitive to the phase quantisation. In other words, near maximum gain results are achieved by co-phasing signals within ±22.5° of each other, or a 45° spread.

The array operates either in receive or transmit mode. In the receive mode, there is a single transmitter (within the volume of the receiver array) and multiple received signals from individual array nodes are centrally processed using EGC. In the transmit mode, each array node transmits a signal with additional phase adjustment determined by the EGT algorithm, such that the received signal amplitude is maximised at a single receive location (within the volume of the transmit array). The first case represents a single-input/multiple-output (SIMO) system, whereas the latter case is a multiple-input/single-output (MISO) system.

2.2 Spectrum analyser and mechanical phase shifters (MISO)

The centralised MISO array was composed of a signal generator that fed radiating antenna elements. A 1:8 power divider split the power evenly across the transmit array elements, and mechanical phase shifters allowed phase adjustment of the signal at each element independently. The mechanical phase shifters provided a tunable phase shift range of a full 360°, with a maximum insertion loss of 0.7 dB at 2.4 GHz (Advanced Technical Materials Inc., Part 2213 [Mention of any company names serves only for identification, and does not constitute or imply an endorsement of such a company or of its product by NIST] [27]). At 750 MHz, the tunable range of phase shift is <150°, so this MISO setup was used only for the 2.4 GHz case. Fig. 1 shows a diagram of the 2.4 GHz measurement setup. Phase adjustment was implemented as described in [18].

A method of selecting transmit array elements was provided by electromechanical relays and selector switches (not shown). The output from each phase shifter was either fed into an antenna element via a 36.6 m RF cable or terminated in 50 Ω load. (The cable loss was ~20 dB.) One of the eight output ports from the power divider was terminated in 50 Ω load connected to a phase shifter for all measurements, since only seven array elements were used in these experiments. Monopoles mounted on aluminum octagon ground planes with an approximate centre-to-vertex measurement of 0.24 m were used for the 2.4 GHz antennas. The ground planes were supported by 1.9 cm diameter polyvinyl chloride (PVC) stands at a height of approximately 1.3 m. (Note: the measurement system connected to the array elements via RF cables to achieve stable phase synchronisation between the array elements. Methods for achieving phase synchronisation between wireless devices are not part of this research, but would be a topic for future work.)

The performance of the centralised array is measured by placing a receive antenna either within the volume of the array or in the vicinity of the array boundary. The receiving antenna, identical to the transmitting array element antennas, was connected to a spectrum analyser via an 18.3 m RF cable, and the measured received power value was obtained by reading the value displayed on the spectrum analyser. Depending on how rapidly the channel changed and on the level of the received signal above the noise floor, the waveform displayed on the analyser exhibited variable rates of fluctuation. However, since the intent of these experiments is not to obtain a precise measurement of the absolute received signal power, but rather to quantify the amount of gain possible by applying the centralised array concept, the precision of visual observation and recording of the power values were deemed adequate. Consistency of results from this manual approach with the automated data capturing system described below for the SIMO case confirms that the manual measurement approach

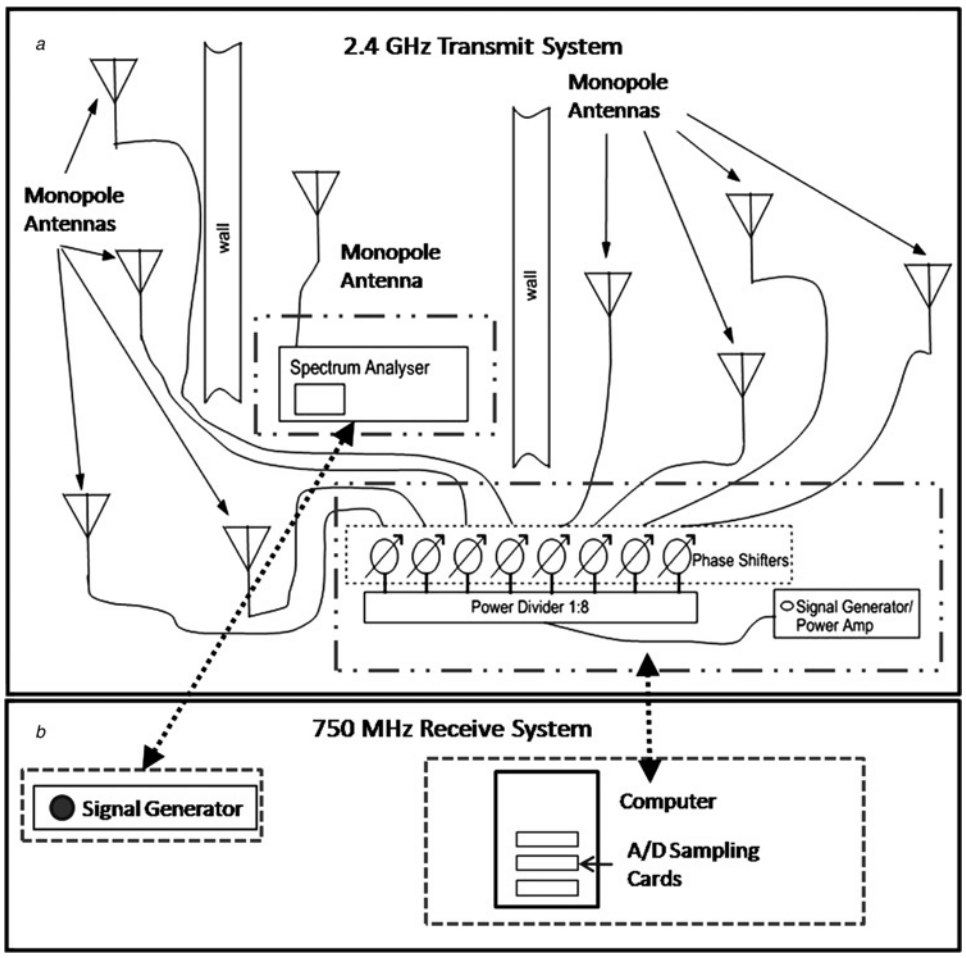

Fig. 1 *Experimental setup for measurements*

For 2.4 GHz (MISO)

a Includes a signal generator, power divider and mechanical phase shifters connected to transmitting monopoles, with a single monopole connected to a spectrum analyser

For 750 MHz (SIMO)

b Show the signal generator now transmitting via a single monopole, and multiple receive monopoles connected to the computer with *A*/*D* sampling cards; phase shifting is done in post processing the samples

provided sufficient accuracy. We comment on small-scale fading because of multipath propagation for each of the individual tests subsequently.

Next, we provide a mathematical description of this MISO system, followed by some implementation particulars of the transmitting and receiving components of the system. The mathematical description here differs from the analysis based on approximate boundary conditions used in [17–19], and is intended to provide a more intuitive description for communication system engineers. A good discussion on MISO and SIMO systems in wireless channels is found in [25]. In the section on experimental results, we also show that computer simulation results that employ recent channel modelling data [26] yield results that agree fairly well with the experimental results. Note that other established indoor models might also provide a reasonably accurate description of the array performance. These models are generally 'site-specific', so care must be taken in selecting the appropriate model. For example, the classic paper by Saleh and Valenzuela [28] pertains mostly to office-type buildings, which will yield much different results from those in, say factories [29], or hospitals [30]. A ray tracing model is also appropriate for indoor environments.

In the MISO field tests, N transmit antennas were used to send a signal to one receive antenna, ($N = 7$ for the MISO tests). The source transmit signal was

$$s(t) = A\cos(\omega_c t) \tag{1}$$

where without loss of generality, we let the phase of the sinusoid be zero and $\omega_c = 2\pi \times 2.4 \times 10^9$ rad/s. The total input signal has an average power $P_S = A^2/(2Z)$ (in watts for A in volts and impedance Z in ohms). As is conventional, for simplicity of signal analysis, we let $Z = 1\ \Omega$. This signal was split approximately equally via a power splitter, followed by a mechanically adjustable phase shifter on each of the N branches, which is connected to the N transmit antennas. Thus, each transmit antenna had an input power of $P_S'/N = (A')^2/(2N)$, where the primed values of P_S and A include losses associated with the power splitter, phase shifters and the connecting cables, essentially equal for all transmit antennas. The signal input to the ith antenna is then

$$S_i(t) = a_i \cos\left(\omega_c t + \psi_i + \varphi_i\right) \tag{2}$$

where $a_i = A'/\sqrt{2N} =$ constant and the phases $\{\psi_i\}_{i=1}^{N}$ are

doi: 10.1049/iet-map.2012.0717

because of splitter, cable and connector delays. Note that for these tests, the key conditions are that ψ_i is constant and that the maximum of s_i is approximately equal for all antennas. The phases $\{\varphi_i\}_{i=1}^{N}$ are the adjustable phases set by the phase shifters, and are used to remove the phase differences because of the different propagation path lengths between transmit and receive antennas in order to achieve the maximum received signal at the receiver. Each signal of the form of (2), when output from the antenna, incurs a gain scaling and a phase shift as a function of elevation and azimuth angles. For any given elevation and azimuth angle, we can incorporate the phase shift into the constant phase, ψ_i, and can similarly incorporate the gain into a_i.

Measurements were taken at two different sites, one on the NIST Campus in Boulder, CO and the other in downtown Denver, CO. The measurements at the NIST site in Boulder, CO encountered minimal object movement within the array area, that is, people, and all the receive antenna test locations were indoors. At the Denver site, there was sporadic pedestrian motion in the environment, and slow vehicular motion outside on the streets. The receive antenna was indoors for all the Denver test cases, except the first location. Thus, for simplicity, we approximate the channel as time invariant. For the sinusoidal signals of (2), we can employ the bandpass channel impulse response (CIR), given by Young *et al.* [19]

$$h_i(\tau) = \sum_{k=1}^{L_i} \alpha_{ki}\delta(\tau - \tau_{ki}) \tag{3}$$

where i indexes the channel from the ith transmit antenna to the receiver, L_i is the number of multipath components (MPCs) in the ith CIR, and the amplitude of the kth MPC in the ith CIR is α_{ki}. The δ is a Dirac delta function and τ_{ki} represents the delay of the kth MPC of the ith CIR. We can employ values for the MPC amplitudes from measurements, but these will be only approximate. Generally models consider the α's to be drawn from a random sample with statistics specified by a large number of measurements. This is discussed further in the description of our computer simulations.

Because the channel is linear, the output of the receive antenna because of the ith transmit signal is given by the convolution of (2) and (3); that is

$$\begin{aligned} r_i(t) &= s_i(t)^* h_i(t) \\ &= a_i \sum_{k=1}^{L_i} \alpha_{ki} \cos\left[\omega_c(t - \tau_{ki}) + \psi_i + \varphi_i\right] \\ &= a_i \sum_{k=1}^{L_i} \alpha_{ki} \cos\left(\omega_c t + \theta_{ki} + \varphi_i\right) \end{aligned} \tag{4}$$

where $\theta_{ki} = \psi_{\mathrm{i}} - \omega_c\tau_{ki}$ can be considered the aggregate channel phase term. The total signal at the receiver is the sum of the N transmitted signals

$$r(t) = \sum_{i=1}^{N} r_i(t) = \sum_{i=1}^{N} a_i \sum_{k=1}^{L_i} \alpha_{ik} \cos\left(\omega_c t + \theta_{ki} + \varphi_i\right) \tag{5}$$

Link distances were approximately 3–50 m. The channel phase terms are $\psi_{\mathrm{i}} - 2\pi \times 2.4 \times 10^9\, \tau_{ki}$. For these link distances, line-of-sight (LOS) values of τ_{ki} range from approximately 10–150 ns, and are larger for reflected signals. Based on this range of values of delay, the channel phase terms span the range of many multiples of 2π. Thus, representing these phases $\{\theta_{ki}\}$ as random and uniformly distributed on the range $[0, 2\pi]$, which is a very good model. The phase shifter phases $\{\varphi_i\}_{i=1}^{N}$ were adjusted to maximise $|r(t)|$.

2.3 Computer with channel sampling cards (SIMO)

The 'reciprocal' approach to the MISO scheme, namely using one transmitter and multiple receiving nodes in a centralised array manner, that is, a SIMO system, can also provide similar signal gains. The SIMO system used in the field tests supported automated data capturing with the centralised array operating in receive mode. In this set of tests, a single transmit antenna was used to send a signal to N receive antennas, where $N = 1, 2, \ldots, 6$. The transmitted signal is in the same form as (1), but the frequency was $f_c = 750$ MHz. Here, we have N individual received signals, each of the form of (4), but without the φ_{i} term – this is now introduced at baseband, where the phase alignment process occurs. Each received signal was down converted and sampled in a separate hardware channel. The individual received signals were then combined at baseband to maximise the amplitude $|r(t)|$ via adjustment of the phases, analogous to the procedure for the MISO tests (see [18]). The complex baseband equivalent of (5), with the inclusion of φ_{i}, is

$$\tilde{r}(t) = \sum_{i=1}^{N} a_i \sum_{k=1}^{L_i} \alpha_{ik}(t) e^{j\left[\theta_{ik}(t) + \varphi_i\right]} \tag{6}$$

The amplitudes and channel phases in (6) are represented here as slowly varying functions of time because of the (slowly) time-varying behaviour of the channel.

The fixed transmitter setup included a signal generator outputting a single frequency at 750 MHz, an 18.5 m cable and a loaded dipole antenna mounted on the same ground plane as used for the 2.4 GHz antennas. The output power on the signal generator was set to 20 dBm, the cable loss was approximately 6 dB and the gain of the antenna approximately 3 dBi. The antenna and the ground plane were supported by a PVC stand at a height of approximately 1.3 m.

This automated data capture setup utilised computer cards that simultaneously sampled six channels directly at 750 MHz, converted the sampled channels to baseband, and then performed the EGC algorithm on the six down converted channels. A raw sample period of 1 ns was used to capture 8192 instances of the six channels, for a total capture time of 8.192 µs. These 8192 samples were converted to baseband, and averaged to obtain a single measurement of the received signal for each channel, which was then used in the MRC algorithm. Each of the six receiver channels was connected via a 36.7 m RF cable to one element of the SIMO array. Each element consisted of an antenna, ground plane and PVC stand identical to that for the fixed transmitter setup.

In this approach, there are six fixed receive elements and a single fixed transmitter. Owing to frequency limitations of the cards, this test was only performed at 750 MHz. The specific cards used in the experiments are the CompuScope 21G8 [31].

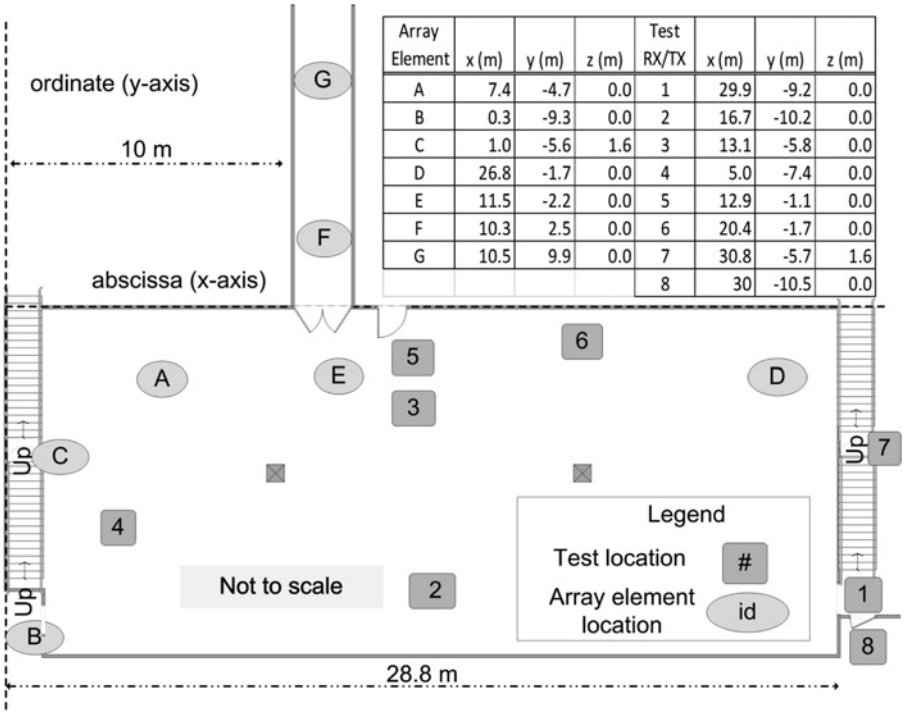

Array Element	x (m)	y (m)	z (m)	Test RX/TX	x (m)	y (m)	z (m)
A	7.4	-4.7	0.0	1	29.9	-9.2	0.0
B	0.3	-9.3	0.0	2	16.7	-10.2	0.0
C	1.0	-5.6	1.6	3	13.1	-5.8	0.0
D	26.8	-1.7	0.0	4	5.0	-7.4	0.0
E	11.5	-2.2	0.0	5	12.9	-1.1	0.0
F	10.3	2.5	0.0	6	20.4	-1.7	0.0
G	10.5	9.9	0.0	7	30.8	-5.7	1.6
				8	30	-10.5	0.0

Fig. 2 *Array element layout and test locations in the Building 24 basement*
All measurements listed are in metres, referenced from the *x*- and *y*-axes

3 Building structure descriptions and experimental setup

This section briefly describes the two building structures and the experimental setup. Although the locations of the array elements were essentially arbitrary, the general locations of elements were chosen to test possible emergency responder field-deployment configurations.

3.1 NIST Building 24, Boulder, Colorado

Building 24 on the NIST, Boulder campus is a combination laboratory and office structure. The structure is composed of typical building materials, including concrete, steel, drywall and acoustic ceiling tiles. The array tests were carried out in a large, open room in the basement, a connected hallway on the same level, landings in two stairwells that connected the basement to upper floors and a small basement bathroom. Fig. 2 shows the layout of the centralised array elements and the test locations, and Table 1 lists whether or not a LOS exists between the *ad-hoc* array elements and test location pairings. Test locations represent either a receive antenna connected to the spectrum analyser for the 2.4 GHz MISO measurements or a transmit antenna connected to the signal generator for the 750 MHz SIMO measurements. Note that array element *E* is not used in the sampling cards and computer data collection, as the system only has six available channels.

3.2 555 17th street, Denver, Colorado

The 555 17th Street location ('Denver site') is an atrium or enclosed lobby area between two buildings in downtown Denver. The structural construction materials are a typical high-rise combination of concrete, glass and steel, and the lobby area consists primarily of stone, glassand metal frames. The layout of the array elements and the test locations both within the atrium and on the sidewalk adjacent to the building are shown in Fig. 3; Table 1 lists LOS pairings.

4 Measurement and simulation results

The experimental results for Building 24 and the Denver site are provided for both measurement systems in the layouts and test locations described previously. The computer system with the network cards allows the collection of a much greater amount of data over a given time period. However, overall results show consistent behaviour between the two

Table 1 LOS matrix

Test location	*Ad-hoc* array element						
	A	*B*	*C*	*D*	*E*	*F*	*G*
Basement							
1	*Y*	*N*	*N*	*N*	*Y*	*N*	*N*
2	*Y*	*N*	*N*	*Y*	*Y*	*N*	*N*
3	*Y*	*Y*	*N*	*Y*	*Y*	*N*	*N*
4	*Y*	*N*	*N*	*Y*	*Y*	*N*	*N*
5	*Y*	*N*	*N*	*Y*	*Y*	*N*	*N*
6	*Y*	*N*	*N*	*Y*	*Y*	*N*	*N*
7	*N*	*N*	*N*	*N*	*N*	*N*	*N*
8	*N*	*N*	*N*	*N*	*N*	*N*	*N*
Denver							
1	*Y*	*Y*	*Y*	*N*	*N*	*N*	*N*
2	*N*	*N*	*N*	*Y*	*Y*	*Y*	*Y*
3	*N*	*N*	*N*	*Y*	*Y*	*Y*	*Y*
4	*N*	*N*	*N*	*Y*	*Y*	*Y*	*Y*
5	*N*	*N*	*N*	*Y*	*Y*	*Y*	*N*
6	*N*	*N*	*N*	*Y*	*Y*	*Y*	*N*
7	*N*	*N*	*N*	*Y*	*Y*	*Y*	*Y*

A '*Y*' indicates LOS between the test location and the array element; '*N*' means non-line-of-sight

doi: 10.1049/iet-map.2012.0717

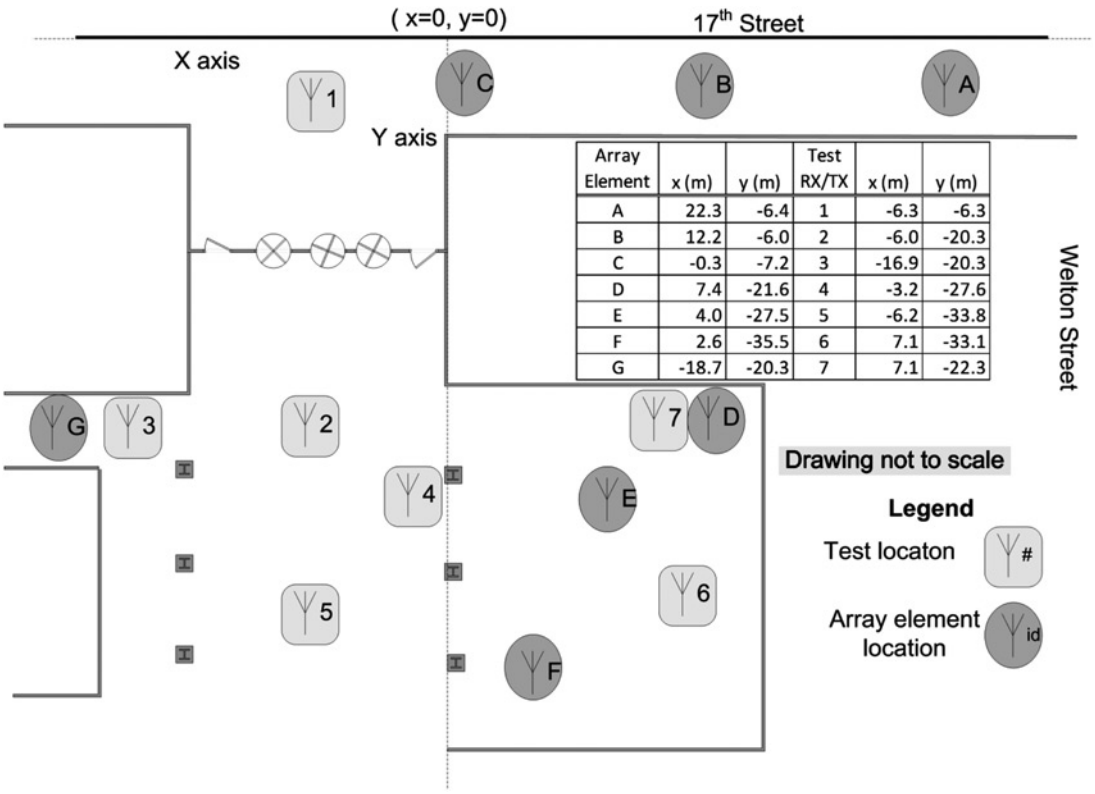

Fig. 3 *Array element and test location layout for the Denver site*
All measurements are in metres, referenced from the *x*- and *y*-axes

approaches, and both validate the centralised array concept. In addition, the computer system allows investigation of the effects because of the co-phasing step increments. We first present the MISO experimental results, followed by the MISO simulation results for comparison; then, the SIMO experimental results.

The combined systematic and random errors introduced by our measurement equipment are expected to be on the order of tenths of decibels. For the 750 MHz test, an automated system was used and either fifty or hundred data sets were collected at each test position. The total received power, after the EGC processing step, had Type A (i.e. statistical) uncertainty of 0.5 dB (see Appendix II in [32]). This variability is attributed to propagation channel changes caused by minor object movement during the experiments. Although no statistical data sets were obtained for the 2.4 GHz measurement, the uncertainties in both sets of experiments are believed to be less than 1 dB. The 2.4 GHz uncertainty estimate is a Type B uncertainty based on previous laboratory measurements and observations of the channel variability during the experiment.

4.1 Spectrum analyser measurement results

Figs. 4*a* and *b* show the EGC results for the 2.4 GHz case, or the transmit (MISO) mode, where the data are normalised with respect to the strongest contributing element. Thus, the initial single element starts at 0 dB for all test positions. In the Building 24 case (Fig. 4*a*), from one to seven transmitting elements were used for all eight of the receiving or test locations. At the Denver site (Fig. 4*b*), from one to seven transmitting elements were used for five of the test locations, and from one to six transmitting elements were used for the remaining two test locations (test locations 3 and 7). In the case of test location 3, array element *G* was not included, since its close proximity could dominate overall performance by a single element. At test location 7, array element *D* was not included for the same reason. Both of these cases represent conditions, where the array would be unnecessary, since there is a very strong signal emanating from a single nearby node.

The results for Building 24 in Fig. 4*a* indicate an increase of 1–6 dB, when the second array element is included. The 6 dB increase is at the theoretical upper bound, assuming identical gain patterns and identical channel path losses from antennas at the test location. (Note that the theoretical upper limit for normalised power in free space is an N^2 curve. Thus, for four elements, the maximum theoretical power gain would be 12 dB, and 16.9 dB for seven elements, assuming equal contributions from the elements at the test location.)

For the Denver site results shown in Fig. 4*b*, at test locations 4 and 6, the gain from two elements is 6.3 and 6.1 dB, respectively. This would appear to be a violation of the theoretical maximum; however, that maximum does not take the environment into account. Many of the array elements are near objects that impact the antenna gain patterns, and link distances are not all identical. Thus, we do not expect identical performance from each array element. In addition, the measurement uncertainty for this type of experiment can be expected to be within 1 dB.

One of the important factors for a practical system is determining the number of array elements to utilise. Fig. 4*a* indicates that the gain increase from one to four elements ranges between 2 and 10 dB. However, the increase from four to seven elements only provides an increase of approximately 1 dB. In Fig. 4*b*, the gain increase from one to four elements ranges between 5.5 and 10 dB. Similar to

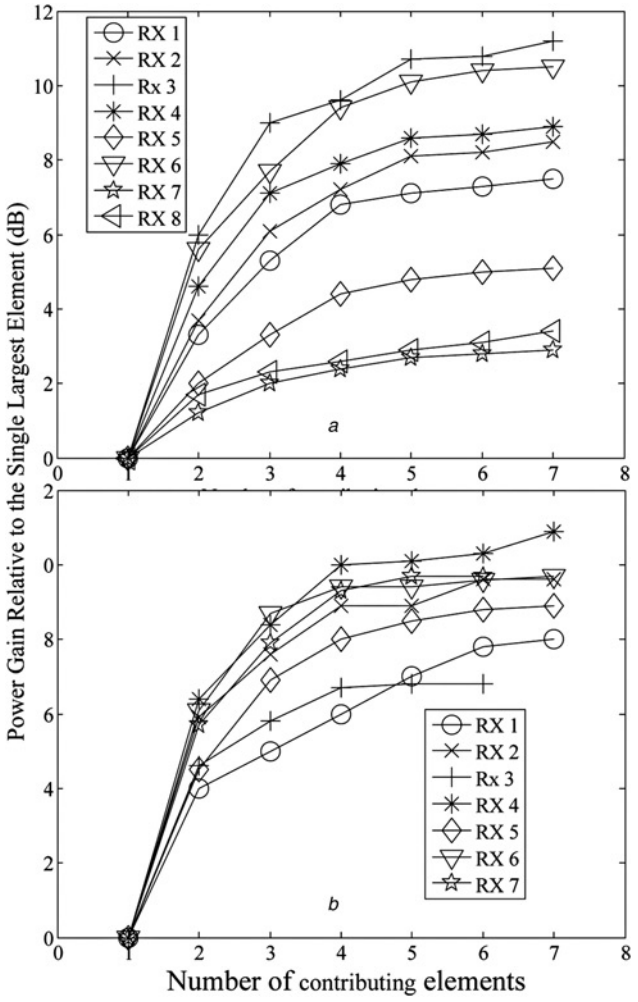

Fig. 4 *Cumulative sum of EGT power (MISO) normalised by the largest contributing element for 2.4 GHz measurements*

a Building 24
b Denver
Different curves denote the different receiver locations (eight locations in (a) Buildings 24 and 7 in (b) Denver)
Two cases in (b) Denver, RX 3 and 7 only include six transmitting elements

the results in Fig. 4*a*, the increase from 4 to 6 or 7 elements only provides about a 1 dB increase. Thus, while the Building 24 case shows a wider range of gain at four array elements, both the Building 24 and the Denver site results show very similar behaviours on a potential practical upper limit of four elements.

4.2 MISO simulation results

Our simulation (in MATLAB®) uses the model described in (4) and (5). For the channel model, we need to specify the number of MPCs [L in (4)], their amplitudes [α's in (4)] and their delays [τ's in (4)]. For this, we used measurement results of a related measurement campaign [26]. In [26], for measurements taken near the Denver site, we found that – as in much of the communications literature, for example, [10] – the channel is most efficiently modelled as random. Running the simulation over multiple trials allows us to gather statistics on achievable MISO gains in this environment, and also implicitly generalises results to other similar (but not identical) settings.

Measurement results from [26] indicate that the number of MPCs L is best modelled as a modified uniform random variable, with probability mass function given by

$$\Pr(L=m) = \begin{cases} \dfrac{1-p_0}{L_{\max}-L_{\min}}, & m = L_{\min}, L_{\min}+1, \ldots, L_{\max}-1 \\ p_0, & m = L_{\max} \end{cases} \tag{7}$$

where the parameters are $p_0 = 0.262$, $L_{\min} = 3$ and $L_{\max} = 21$. Thus, the probability mass function is equal to 0.262 for $L = 21$, and equal to 0.041 for L equal to integers from 3 to 20. For each trial of the simulation, we generate a unique value of L for each of the N channels.

The MPC delays were found to be exponentially distributed, with probability density function

$$p_\tau(\tau) = \exp(-\tau/v)/v \tag{8}$$

where here $v = 340.6$ ns. As with variable L, we select each of the L MPC delays for each of the N channels from this distribution.

Finally, for the MPC amplitudes, these also follow an exponential distribution; specifically, we found the best fit

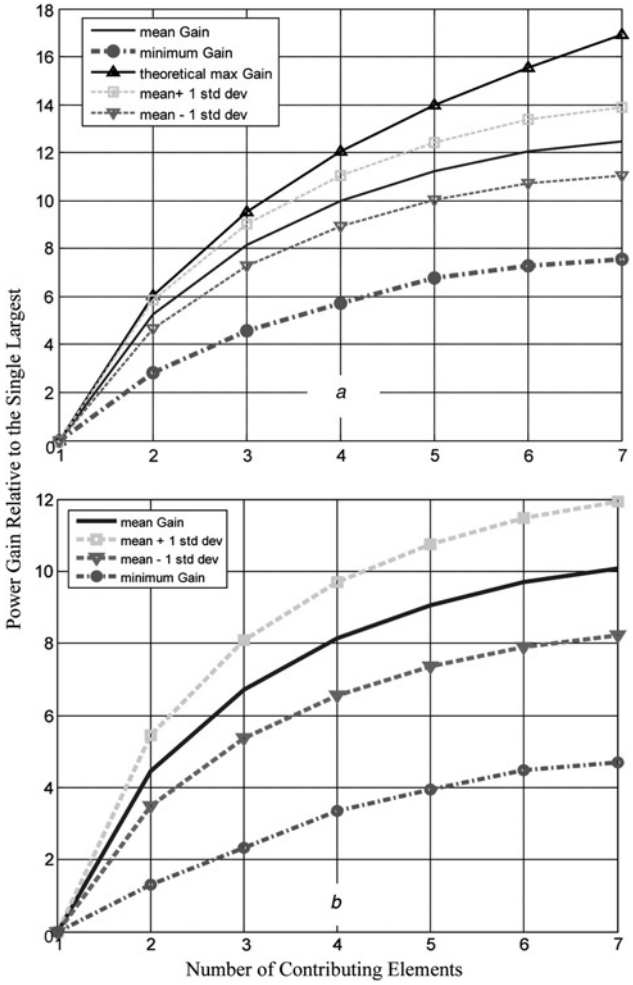

Fig. 5 *Simulated MISO gain statistics*

a Denver channel model
b Denver channel model with the random path loss model included

doi: 10.1049/iet-map.2012.0717

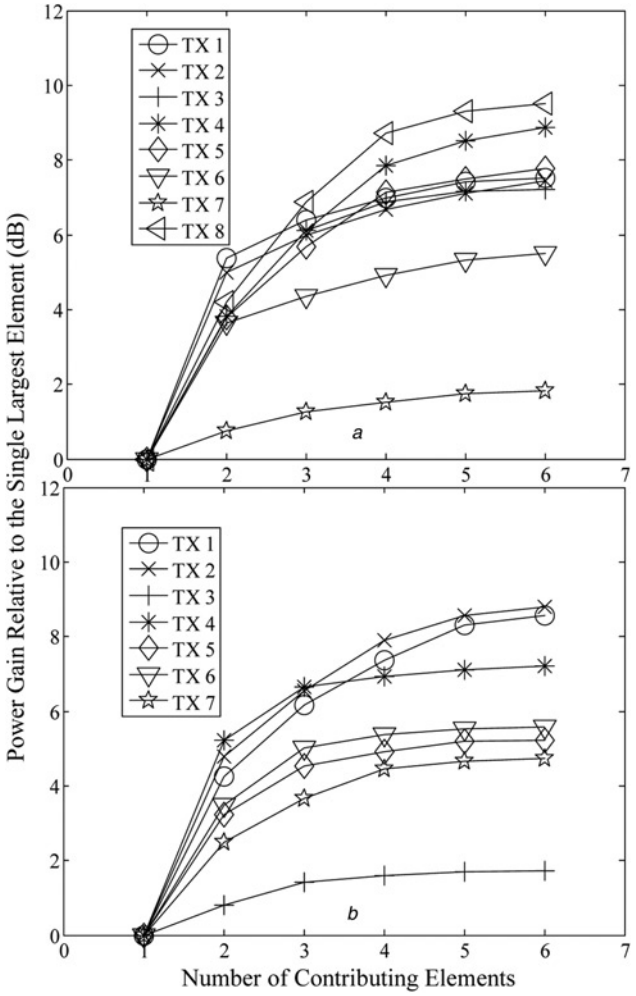

Fig. 6 *Average cumulative power results normalised by the largest contributing element, at 750 MHz (SIMO)*

a Building 24 based on 41 data sets
b Denver based on 71 data sets
TX number refers to the transmitter position, which is the same as the RX position used in the spectrum analyser measurements

function for (normalised) power against delay to be

$$P_\tau(\tau) = c_0 \exp(-c_1 \tau) \tag{9}$$

with $c_0 = 1$, $c_1 = 0.076$. Thus, for each of the N channels, the L unique amplitudes are drawn from this distribution, mapping via $\alpha_i = \sqrt{P_i} > 0$.

For each simulation trial, we first generate the N channel models as described; then, implement the co-phasing algorithm, and finally record gains against the number of included antenna elements. Given the channel model, for any given simulation run, the powers and delays of the MPCs can yield both constructive and destructive combining as the transmitter phases are varied. The co-phasing algorithm is 'blind' to this fact although, and simply adjusts phases to maximise received power. This 'blindness' is a virtue, since it keeps the algorithm simple – trying to adjust phases to compensate for the large number of potential MPCs would be impractical (although this could be done in adaptive systems, much as a rake receiver implements MRC in spread-spectrum systems [12]).

Results of the MISO simulation are shown in Fig. 5*a*, in the same format as in Fig. 4. Fig. 5*a* shows maximum, minimum and mean gains achieved over 100 trials of the simulation. We also show the mean gain ±1 standard deviation, to indicate a range of values that might be attained in practice in this type of environment. Comparing simulation results to the measured results of Fig. 4*b*, we see reasonable agreement overall. The simulated mean gains roughly follow the experimental means for $N = 2$ and 3 elements, but exceed the experimental maxima for N larger than five elements. The range of gains for $N = 2$ and 3 agrees well with the measured results.

Our second simulation result, Fig. 5*b* shows a similar plot, using the same multipath channel model, but in addition we include large-scale propagation path loss. In [31], propagation in the environment was found to be well modelled by a d^{-n} law, with d = distance and n = propagation path loss exponent. This exponent was modelled as uniform between 1.9 and 3.6. Fig. 5*b* shows the simulation results after adding this feature, where we have omitted plotting the theoretical maximum curve. Comparing with the previous figure, we see that the minimum gain values are smaller, as are the mean gain values. The curves for the simulated mean gains ±1 standard deviation bound fairly well the range of gains attained in the experiment, shown in Fig. 4*b*, indicating that the inclusion of path loss in the multipath channel model improves agreement between simulations and measurements.

Thus, the simulation results do indeed corroborate the measured results. Discrepancies between simulations and measurements are attributable to multiple factors, including imperfect antenna gain patterns, unaccounted for fixed losses through walls, a simulated mean delay [$v = 340.6$ ns in (8)] that is likely larger than actual delays, etc. Nonetheless, agreement between simulations and measurements is good, particularly for smaller values of N.

4.3 Channel sampling card measurement results

The data collection and subsequent application of the co-phasing algorithm to the 750 MHz SIMO signals provides results consistent with the data at 2.4 GHz discussed above. The outputs from the co-phasing algorithm are then averaged to compare with the 2.4 GHz results.

Averaging of several samples from the previous results for the sampling cards allows a more direct comparison to the spectrum analyser measurements. In Figs. 6*a* and *b*, normalised power is plotted against the number of array receiving elements for Building 24 and the Denver site, respectively. These values are computed by averaging 41 data sets for the Building 24 data and 71 data sets for the Denver site (these data ranges were chosen to avoid including any data collected during the off/on and on/off transitions of the transmitter). A true direct comparison is not possible, since the spectrum analyser results are for 2.4 GHz and the sampling card results are for 750 MHz. However, similar to the spectrum analyser MISO results, for most of the test positions, the gain is between 2 to 6 dB, when the second element is included and the rate of gain increase beyond four elements drops significantly.

Test position three for the Denver site shows less than 2 dB of gain even at six array elements, because of the close proximity of the transmitter and the receiving array element located at *G*. (Recall that this array element was not included in the spectrum analyser data for test position 3.) Test position 7 in Building 24 behaves nearly the same with

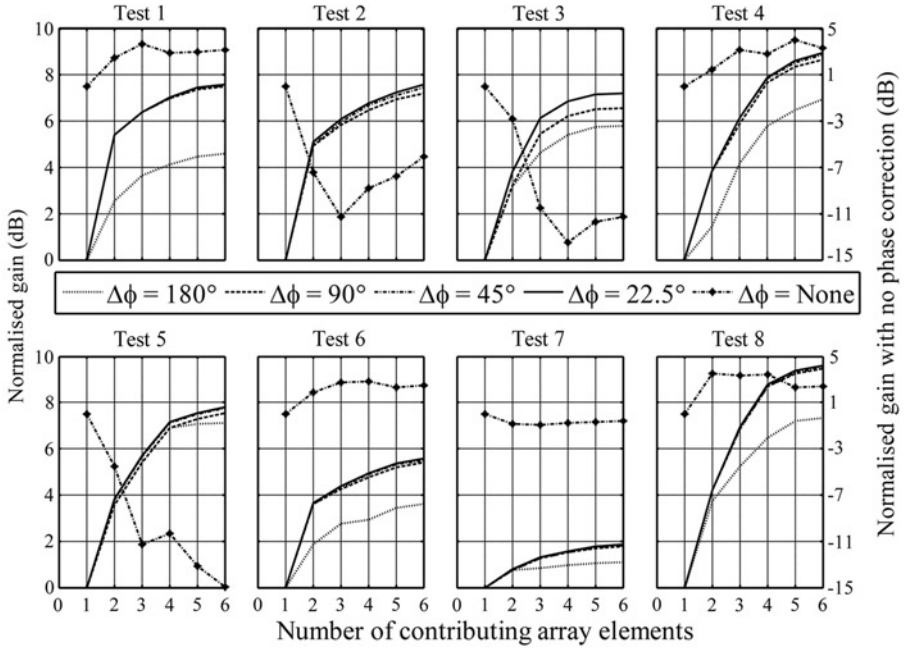

Fig. 7 *Building 24 site*

750 MHz gain results for per test location.
The left vertical axis covers a range from 0 to 10 dB, and corresponds to the phase steps from 22.5 to 180°
The right vertical axis ranges from −15 to 5 dB, and corresponds no phase correction (the signals are directly combined without using the MRC algorithm)
The test number is the test location

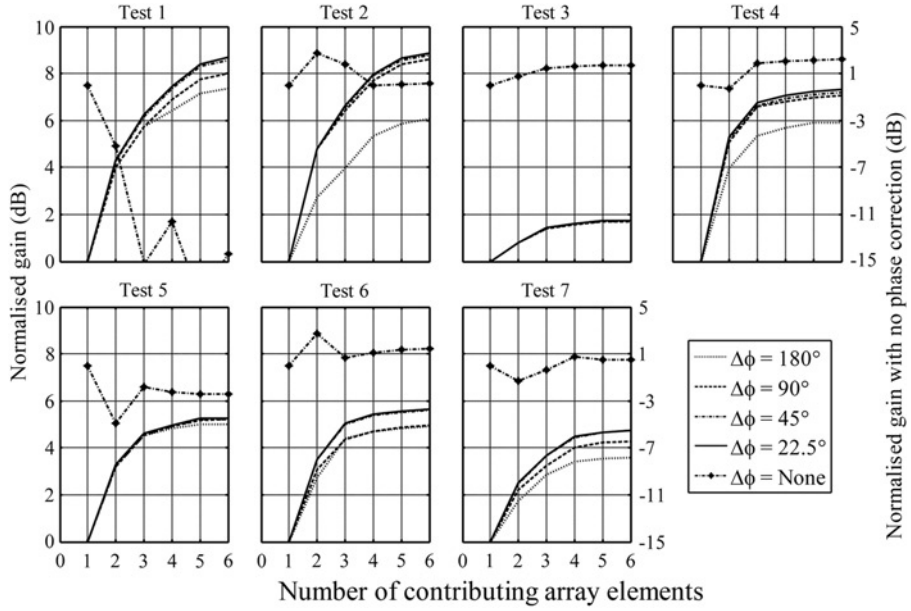

Fig. 8 *Denver site 750 MHz normalised gain results per test location*

The left vertical axis covers a range from 0 to 10 dB, and corresponds to the phase steps from 22.5 to 180°
The right vertical axis ranges from −15 to 5 dB, and corresponds to no phase correction (the signals are directly combined without using the MRC algorithm)
The test number is the test location

both measurement systems, which is likely due to the fact that the test position is elevated above the array plane.

One of the key requirements to such a centralised array system is phase synchronisation between nodes. As evident by Mudumbai [14, 16]; Berger and Wittneben [15], developing algorithms and approaches to provide phase synchronisation in such networks is an active area of research. The 750 MHz system used here provides some measured data as to effects of a less than optimal phase alignment. In Figs. 7 and 8, the gain per test position is calculated for different phase steps. For both Building 24 and Denver cases, the results for phase steps of 90 and 22.5° are within 1 dB for all locations. (Phase step of 90° corresponds to a phase alignment of ±45°.) These measured results are consistent with the assertions in [14, 19] that phase deviates significantly from the optimal, for example,

doi: 10.1049/iet-map.2012.0717

more than 30°, have minimal impact on the gain performance. This was also corroborated by our simulation results (not shown for brevity).

5 Conclusions

The measurement and simulations completed here support the concept of a centralised array of arbitrarily placed nodes to improve the signal strength in buildings by coordinated transmission/reception from/to multiple nodes. Two clear results are that (i) in practice, diminishing returns of the gain appear after the inclusion of four nodes and (ii) a practical phase adjustment increment of ±22.5° achieves near maximum available gain. The combination of these factors implies that a centralised array can be constructed to yield beneficial gain results. These results also provide merit to follow-on research on the optimal method for phase synchronisation between nodes for communication with transceivers within the same building.

This work focused on proving the feasibility of the centralised array concept for public-safety communications in a real-world setting. As part of the efforts, we constructed a measurement system that allowed simultaneous signal collection at multiple, separated locations. We also used measured data to develop a simulation experiment that further corroborated benefits of the centralised array approach. Both the measurement system and the simulation approach have potential applicability towards the understanding of RF propagation behaviour in traditional *ad-hoc* wireless networks, beyond the specific application studied here.

6 Acknowledgments

This work was sponsored by US Department of Justice through the Public Safety Communications Research Laboratory, Derek Orr, Program Manager. The authors thank members of the technical staff of the NIST Electromagnetics Division 818, who pulled together the equipment. The authors also thank Patrick Fine and his staff for providing access to the 555 17th Building in Denver, Colorado.

7 References

1 'Statement of requirements: background on public safety wireless communications, The SAFECOM Program, Department of Homeland Security, Vol. 1, March 10, 2004
2 Worrell, M., MacFarlane, A.: 'Phoenix fire department radio system safety project', Final Report, Phoenix Fire Department October. 8, 2004
3 'National Commission on Terrorist Attacks Upon the United States'. 9/11 Commission Report, 2004
4 New York World Trade Center terrorist attack, Wireless Emergency Response Team (WERT), Final Report for September 11, 2001, October 2001
5 Holloway, C.L., Koepke, G., Camell, D., *et al.*: 'Propagation and detection of radio signals before, during and after the implosion of a thirteen story apartment building', NIST Technical Note 1540, Boulder, CO, May 2005
6 Holloway, C.L., Koepke, G., Camell, D., Remley, K.A., Williams, D.F.: 'Radio propagation measurements during a building collapse: applications for first responders'. Proc. Int. Symp. on Advanced Radio Technology, Boulder, CO, March 2005, pp. 61–63
7 Remley, K.A., Koepke, G., Holloway, C.L., *et al.*: 'Measurements to support broadband modulated-signal radio transmissions for the public-safety sector', NIST Technical Note 1546, Boulder CO, April 2008
8 Kelley, M.R.: 'The spectrum auction: big money and lots of unanswered questions', *IEEE Internet Comput.*, 2008, **12**, (1), pp. 66–70
9 Available at http://www.transition.fcc.gov/pshs/public-safety-spectrum/700-MHz/safetyband.html
10 Molisch, A.: 'Wireless communications' (John Wiley & Sons, 2005, 2nd edn. 2010)
11 Rappaport, T.S.: 'Wireless communications: principles and practice' (Prentice-Hall PTR, 1996, 2nd edn. 2002)
12 Tonguz, O.K., Ferrari, G.: 'Ad-hoc wireless networks' (John Wiley & Sons Ltd., 2006, 1st edn.)
13 Rutagemwa, H., Willink, T.J., Li, L.: 'Modeling and performance analysis of multihop cooperative wireless networks', *IEEE Trans. Veh. Technol.*, 2010, **59**, (6), pp. 3057–3069
14 Mudumbai, R., Barriac, G., Madow, U.: 'On the feasibility of distributed beamforming in wireless networks', *IEEE Trans. Wirel. Commun.*, 2007, **6**, (5), pp. 1754–1763
15 Berger, S., Wittneben, A.: 'Carrier phase synchronization of multiple distributed nodes in a wireless network', IEEE Eighth Workshop on Signal Processing Advances in Wireless Communications, 2007 (SPAWC 2007), Helsinki, Finland, June 2007
16 Mudumbai, R., Brown, D.R., Madow, U., Poor, H.V.: 'Distributed transmit beamforming: challenges and recent progress', *IEEE Commun. Mag.*, 2009, **47**, (2), pp. 102–110
17 Young, W.F., Kuester, E.F., Holloway, C.L.: 'Optimized arbitrary wireless device arrays for emergency response communications', NIST Technical Note 1538, Boulder CO, March 2005
18 Young, W.F., Kuester, E.F., Holloway, C.L.: 'Optimizing arrays of randomly placed wireless transmitters for receivers located within the array volume', *IEEE Trans. Antennas Propag.*, 2007, **55**, (3), pp. 698–706
19 Young, W.F., Kuester, E.F., Holloway, C.L.: 'Measurements of randomly placed wireless transmitters used as an array for receivers located within the array volume with application to emergency responders', *IEEE Trans. Antennas Propag.*, 2009, **57**, (1), pp. 241–247
20 Stuber, G.: 'Principles of mobile communications' (Kluwer Academic Publishers, 1996)
21 Lo, T.K.Y.: 'Maximum ratio transmission', *IEEE Trans. Commun.*, 1999, **47**, (10), pp. 1458–1461
22 Love, D.J., Heath, Jr. R.W.: 'Equal gain transmission in multiple-input multiple-output wireless systems', *IEEE Trans. Commun.*, 2003, **51**, (7), pp. 1102–1110
23 Skolnik, M.I., King, D.D.: 'Self-phasing array antennas', *IEEE Trans. Antennas Propag.*, 1964, **12**, (2), pp. 142–149
24 DiDomenico, L.D., Rebeiz, G.M.: 'Digital communications using self-phased arrays', *IEEE Trans. Microw. Theory Tech.*, 2004, **49**, (4), pp. 677–684
25 Durgin, G.D.: 'Space-time wireless channels' (Pearson Education, Inc., Publishing as Prentice-Hall, Inc., 2003)
26 Gentile, C., Matolak, D.W., Remley, K.A., Holloway, C.L., Wu, Q., Zhang, Q.: 'Modeling urban peer-to-peer channel multipath characteristics for the 700 MHz and 4.9 GHz public safety bands'. Proc. IEEE ICC, Ottawa, Canada, June 2012, pp. 4557–4562
27 Available at http://www.pdf1.alldatasheet.net/datasheet-pdf/view/261103/ATM/P2213.html
28 Saleh, A.A.M., Valenzuela, R.A.: 'A statistical model for indoor multipath propagation', *IEEE J. Sel. Areas Commun.*, **5**, (2), pp. 128–137
29 Rappaport, T.S.: 'Characterization of UHF multipath radio channels in factory buildings', *IEEE Trans. Antennas Propag.*, 1987, **37**, (8), pp. 1058–1069
30 Kyro, M., Haneda, K., Simola, J., *et al.*: 'Measurement based path loss and delay spread modeling in hospital environments at 60 GHz', *IEEE Trans. Wirel. Commun.*, 2011, **10**, (8), pp. 2423–2427
31 Cobra CompuScope 21G8, GaGe CobraTM. Available at http://www.wuntronic.eu/index.php?site=2&xid=65&subid=185&sub2id=186&pid=255
32 Young, W.F., Matolak, D.W., Holloway, C.L., Bikhazi, N., Koepke, G., Fielitz, H.: 'An intra-volume Ad-hoc array concept for improved public-safety communications', NIST Technical Note 1553, Boulder, CO, 2010